Check for updates

ADVANCED FUNCTIONAL MATERIALS
www.afm-journal.de

In Situ Formation of Gel Electrolyte with Enhanced Diffusion Kinetics and Stability for Achieving Fast-Charging Li-Ion Batteries

Xiaofei Liu, Leyi Guo, Zibo Zhang, Jian Wang, Hongzhen Lin, Gaunwu Li, Xing Ou, Dong Wang,* and Weitao Zheng**

In situ formation of gel polymer electrolytes (GPE) has been a promising candidate to address individual limitations of liquid/solid electrolytes and interfacial stability. However, the controllable conversion of liquid electrolyte (LE) precursor to GPE remains a great challenge with lower lithium-ion transport, which is far from the demand for fast-charging properties. Herein, a strategy of gradient polymerization of forming GPE is pioneered, stabilizing the electrolyte/electrode interface with an accelerated Li^+ migration feature. As demonstrated by theoretical simulations and visualization experiment results, the formation mechanism of GPE via a partial inhibitory mechanism of Lithium nitrate ($LiNO_3$) to control the solvent polymerization is comprehensively investigated, exhibiting the preferential interaction between nitrate anion (NO_3^-) and the Lewis acidic site in lithium bis(fluorosulfonyl)imide (LiFSI). Consequently, a stable amorphous GPE with high Li^+ conductivity (5.10 mS cm^{-1}) and an inorganic solid electrolyte interphase (SEI)-dominate layer derived from spectroscopical measurements are achieved on the graphite electrode surface. The as-prepared lithium iron phosphate (LFP)||graphite pouch cell stabilizes the capacity of 109.80 mAh g^{-1} (capacity retention: 80.02%) after 715 cycles at 5 C/1 C (charge/discharge), corresponding to the energy density of 277.64 Wh kg^{-1}. This work provides a facile but practical approach to designing a highly stable GPE for fast-charging lithium-ion batteries.

1. Introduction

Lithium-ion batteries (LIB) with graphite anodes have been widespread applied in commercial energy storage systems such as mobile phones and drones. However, the rapid development of electric vehicles requires batteries with higher energy density and higher power performance. Traditional ethylene carbonate (EC)-based liquid electrolytes have been favored for their high Li-ion conductivity and compatibility with graphite. However, the thermally unstable salts (i.e., lithium hexafluorophosphate, $LiPF_6$) and flammable organic solvents (i.e., carbonates) in liquid EC-based electrolytes heighten the risk of thermal runaway and even fire,[1] particularly under fast-charging conditions due to significant Joule heating. To mitigate these risks, many efforts in electrolyte engineering have been made. For example, adding various types of flame retardant additives in liquid electrolytes, including phosphate esters and fluorinated solvents.[2] Alternatively, solid-state electrolytes (SSEs),

X. Liu, L. Guo, G. Li, D. Wang, W. Zheng
Key Laboratory of Automobile Materials of MOE
School of Materials Science and Engineering
and Jilin Provincial International Cooperation Key Laboratory of
High-Efficiency Clean Energy Materials
Jilin University
Changchun 130013, P. R. China
E-mail: wangdong2023@jlu.edu.cn; wtzheng@jlu.edu.cn

The ORCID identification number(s) for the author(s) of this article can be found under https://doi.org/10.1002/adfm.202408525

© 2024 The Author(s). Advanced Functional Materials published by Wiley-VCH GmbH. This is an open access article under the terms of the Creative Commons Attribution License, which permits use, distribution and reproduction in any medium, provided the original work is properly cited.

DOI: 10.1002/adfm.202408525

Z. Zhang, X. Ou
Engineering Research Centre of the Ministry of Education for Advanced
Battery Materials, School of Metallurgy and Environment
Central South University
Changsha, Hunan 410083, P. R. China

J. Wang, H. Lin
i-lab & CAS Key Laboratory of Nanophotonic Materials and Devices
Suzhou Institute of Nano-Tech and Nano-Bionics
Chinese Academy of Sciences
Suzhou, Jiangsu 215123, P. R. China
E-mail: jian.wang@kit.edu

J. Wang
Helmholtz Institute Ulm (HIU)
D89081 Ulm, Germany

J. Wang
Karlsruhe Institute of Technology (KIT)
D-76021 Karlsruhe, Germany

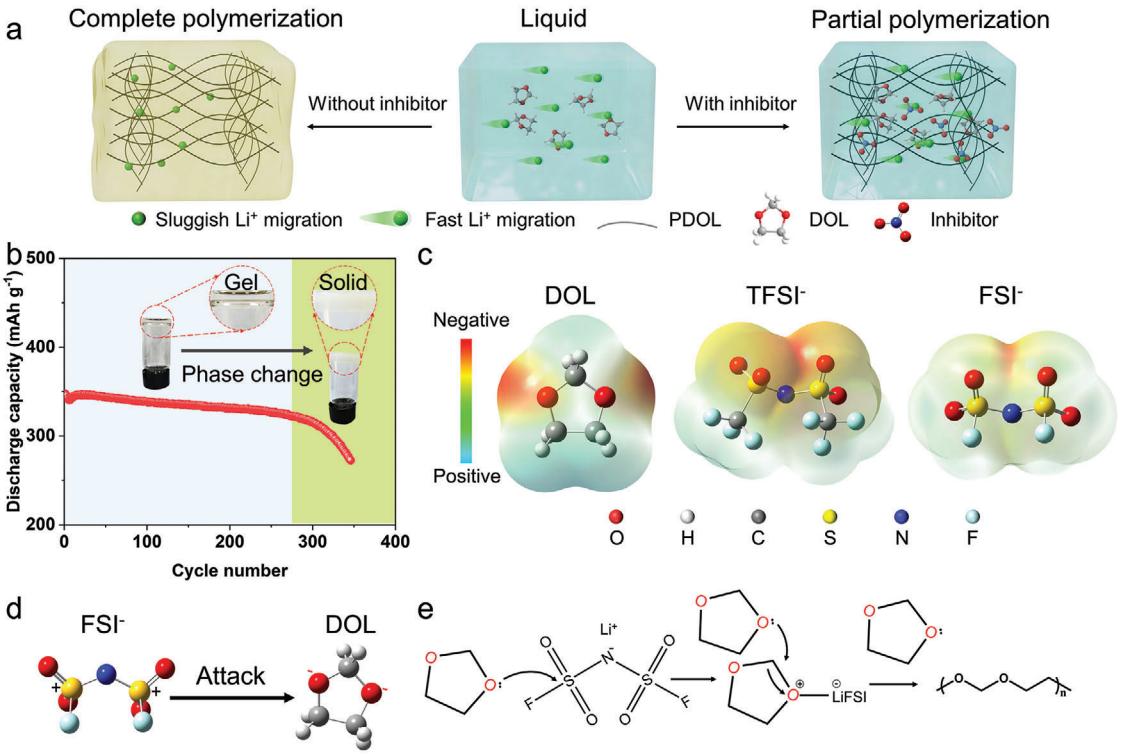

Figure 1. a) Schematic illustration of the polymerization process of precursor liquid electrolyte with or without inhibitor. b) Cycling performance of graphite||Li half cell in GPE (aging two days) at 5 C/1 C (discharge/charge) and optical images of initial GPE after aging for 2 days (gel state) and GPE after aging for 30 days (solid state). c) Electrostatic potential (ESP) images of DOL, $TFSI^-$, FSI^-. d) Proposed interactions of DOL and FSI^-. e) Schematic illustration of the ring-open polymerization of DOL with LiFSI.

including solid polymer electrolytes (SPE), have gained great attention due to their excellent chemical stability, high modulus, and inherent flame-retardant properties,[3] which can effectively address the safety concerns of liquid electrolytes (leakage and combustion).[4] However, the low Li^+ conductivity,[5] poor wettability, and inadequate and loose interfacial contact between SSE/SPE and electrodes lead to high interfacial contact impedance, which severely limits their practical applications in fast-charging batteries.[6]

GPE combines the high modulus of SPE with the high Li-ion conductivity and good wettability of liquid electrolytes, receiving extensive research and attention.[7] To achieve intimate interfacial contact, in situ GPE has been developed due to their good wettability with the active materials and electrodes, reducing the interfacial contact impedance and improving the interfacial compatibility between GPE and electrode. Therefore, various liquid precursor monomers, such as vinyl carbonate (VC),[8] tetrahydrofuran (THF),[9] poly(ethylene glycol) diacrylate (PEGDA),[10] have been employed to form GPE via in situ polymerization. The ether-based 1,3-Dioxolane (DOL) solvent monomer, with low viscosity and mild ring-opening conditions, has been widely employed in the fabrication of GPE via in situ polymerization. To match the lithium-ion transport and polymerization degree, the initiation of initiators, such as $LiPF_6$,[11] aluminum trifluoromethanesulfonate $[Al(OTf)_3]$,[12] LiFSI are designed and investigated.[13] However, the initiators in LE always trigger the ring-opening polymerization of solvent monomer as complete as possible, leading to transformation from LE to SPE as a solidification, which is also accelerated by the formed joule heat. This liquid-solid transformation results in decreased Li^+ conductivity and poor interfacial contact between the electrolyte and the active materials, increasing the interfacial polarization and then deteriorating the performance of the battery.[14] Typically, the cyclic ether DOL monomer in liquid electrolyte (LE: 1 M LiFSI in DOL) precursor can in situ activated by the initiator of LiFSI, the initiator (LiFSI) in LE continuously triggers the consumed and complete polymerization, forming a SPE, which leads to sluggish Li^+ migration and low Li^+ conductivity. Therefore, it is crucial to inhibit this complete solidification evolution to maintain the stability of GPE during operation. Additionally, the weak coordination between DOL and Li^+ facilitates fast Li^+ desolvation, improving the fast-charging performance.[15] Thus, it is of significance to look for a suitable inhibitor that can achieve partial polymerization of LE, forming and building a gradient polymerization of GPE with enhanced ion mobility.

Herein, a strategy of gradient polymerization of forming GPE is pioneered, stabilizing the electrolyte/electrode interface with an accelerated Li^+ migration feature. The stable amorphous gel polymer electrolyte with high Li^+ conductivity (5.10 mS cm^{-1}) is achieved via in situ partial polymerization using $LiNO_3$ inhibitor, improving the Li^+ migration kinetics and stability for fast-charging performance of graphite (**Figure 1a**). The strong Lewis basic NO_3^- in GPELN (LE with 0.05 M $LiNO_3$ after in situ polymerization) can preferentially coordinate with the Lewis acidic site in LiFSI, blocking its attack on the oxygen atom of DOL due to the inhibitory effect of the huge steric hindrance effect for

© 2024 The Author(s). Advanced Functional Materials published by Wiley-VCH GmbH

16163028, 0, Downloaded from https://onlinelibrary.wiley.com/doi/10.1002/adfm.202408525 by Karlsruher Institut F., Wiley Online Library on [01/08/2024]. See the Terms and Conditions (https://onlinelibrary.wiley.com/terms-and-conditions) on Wiley Online Library for rules of use; OA articles are governed by the applicable Creative Commons License

NO_3^-, which inhibits the continual polymerization of DOL and the transformation of LE to SPE. Additionally, $LiNO_3$ also helps to form a stable inorganic substance-dominated SEI to the stability of SEI. Consequently, graphite||Li half cell exhibits outstanding fast-charging cycling performance with in situ GPELN. The as-prepared pouch full cell maintains a reversible capacity of 109.80 mAh g^{-1} after 715 cycles at 5 C/1 C (charge/discharge), corresponding to a capacity retention of 80.02%. This inhibitory effect provides new insights and pathways for stabilizing in situ GPE with high-rate ion transport kinetics.

2. Results and Discussion

The DOL monomer-based GPE is fabricated by in situ polymerization of the precursor liquid electrolyte (LE, 1 M LiFSI in DOL), and the GPE obtains higher discharge capacity than carbonate electrolyte and liquid electrolyte in Figure S1 (Supporting Information), Figure 1b exhibits the typical electrochemical phenomenon of a graphite||Li half cell cycled at 5 C/1 C (discharge/charge). As displayed, two areas of different pristine GPE can only stabilize for ≈280 cycles with small polarization, and then the capacity experiences with sharp decrease with increasing polarization (Figure S2a, Supporting Information). To prove this, electrochemical impedance spectroscopy (EIS) was conducted to analyze the kinetic and resistance changes of the GPE before and after cycling. As shown in Figure S2b,c (Supporting Information), R_{sei} (the impedance of SEI) and R_{ct} (the impedance of charge transfer) significantly increase after 350 cycles, which indicates that the thickness or component of SEI was changed during cycling, impeding Li^+ migration for fast exchange at the interface. Optical experiments were conducted to investigate the relationship between the transformation of electrolytes and electrochemical performance. The inset in Figure 1b shows the optical images of GPE aging for 2 days and 30 days. The GPE without inhibitor transitions from a clarified and transparent state to a white solid-state like SPE after resting for enough time (Figure S3, Supporting Information), indicating the conversion from GPE to SPE. Fourier transforms infrared spectroscopy (FTIR) and nuclear magnetic resonance spectroscopy (NMR) were employed to reveal the molecular structure changes after aging for 30 days. Figure S4 (Supporting Information) illustrated that the peak assigned to DOL almost vanished after aging for 30 days in the ^{1}H-NMR.[16] Meanwhile, the C—O—C vibrational peak located at 1030 cm^{-1} almost disappears in GPE after aging for 30 days,[17] indicating that the GPE after aging for 30 days is essentially composed of long-chain poly(1,3-Dioxolane) (PDOL), which was consistent with the NMR results. These results demonstrate that the DOL in GPE continuously polymerizes to completely form PDOL during the electrochemical processes, leading to the phase transition from LE to SPE, preventing the fast-charging performance due to the sluggish Li^+ migration and huge interfacial impedance of SPE.

To elucidate the internal mechanism from GPE to SPE, the electrostatic potential (ESP) and visualization experiments were performed. The electron in ESP of the DOL monomer molecule is mainly concentrated on the oxygen (O) atom due to its strong electron attraction,[18] and the ESP of bis(trifluoromethanesulfonyl)imide anion ($TFSI^-$) is mainly distributed near the oxygen (O) and nitrogen (N) atoms (Figure 1c). The corresponding visualization experiments demonstrate that the liquid electrolyte (1 M lithium bis(trifluoromethanesulfonyl)imide (LiTFSI) in DOL) does not form GPE after aging for 30 days (Figure S5a, Supporting Information), which strongly indicates that LiTFSI can't induce ring-opening polymerization of DOL. Although the sulfur (S) atom in the $TFSI^-$ can be a Lewis acidic site due to its electron-deficient feature,[19] the attached CF_3 functional group creates significant steric hindrance, inhibiting interactions with DOL and suppressing the ring-opening polymerization of DOL.[20] However, the CF_3 functional group in $TFSI^-$ is replaced with a fluorine (F) atom to form bis(fluorosulfonyl)imide anion (FSI^-), which is significantly different from $TFSI^-$. The visualization experiment obviously shows that the LE (1 M LiFSI in DOL) forms a clarified and transparent GPE after two days (Figure S5b, Supporting Information), which firmly demonstrates that FSI^- can attack the DOL and induce in situ ring-opening polymerization. The electronic density in ESP of FSI^- is mainly concentrated on the O and N atoms, while the S atom exhibits an electron-deficient center. And F atom leads to a minor steric hindrance effect, this configuration enables the S atom to serve as a strong Lewis acidic site, effectively attacking the Lewis basic O atom in DOL and triggering the ring-opening polymerization of DOL (Figure 1d).

To ascertain the steric hindrance effect and interaction between the electron-deficient S atom and the DOL solvent, the ESP of 1,3,2-dioxathiolane 2,2-dioxide (DTD) is calculated in Figure S5c (Supporting Information). The electronic density in ESP is primarily concentrated around the O atom, with the S atom exhibiting an electron-deficient center. Additionally, DTD also exhibits a smaller steric hindrance effect than $TFSI^-$ and FSI^-, the S atom forms a strong Lewis acidic site like that in the FSI^-. Therefore, 0.1 M DTD is introduced into the liquid electrolyte (1 M LiTFSI in DOL with 0.1 M DTD), and the gel electrolyte is obtained after 2 days (Figure S5c, Supporting Information), which demonstrates that the S atom in DTD acts as a Lewis acidic site to trigger ring-opening polymerization of DOL.[18] These results indicate that the S atom in LiFSI acts as a strong Lewis acidic site, triggering the polymerization of DOL as schematically illustrated in Figure 1e. LiFSI, an integral part of the GPE, acts as an initiator, leading to the polymerization of DOL and ultimately facilitating the transition from LE to SPE (Figure 1b). Nearly all DOL has polymerized into PDOL in SPE, severely reducing the Li^+ conductivity.[21] The highest occupied molecular orbital (HOMO) and lowest unoccupied molecular orbital (LUMO) of different long-chain PDOL (Figures S6–S8, Supporting Information) show that the HOMO and LUMO energy decrease with the PDOL molecular chain length increases (Figure S8, Supporting Information), which indicates that long-chain PDOL is more prone to gain reduction on the graphite surface,[10] increasing the interface impedance. These results also indicate a decrease in interfacial stability and an increases in interfacial impedance. Consequently, it is essential to develop an effective strategy for inhibiting the continual polymerization of DOL and the evolution from LE to SPE.

As depicted in Figure 1d, the S atom in FSI^-, acting as a strong Lewis acidic site, attacks the O atom in DOL, triggering the ring-opening polymerization of DOL.[13a] Therefore, blocking this attack will help to inhibit the ring-opening

© 2024 The Author(s). Advanced Functional Materials published by Wiley-VCH GmbH

16163028, 0, Downloaded from https://onlinelibrary.wiley.com/doi/10.1002/adfm.202408525 by Karlsruher Institut F., Wiley Online Library on [01/08/2024]. See the Terms and Conditions (https://onlinelibrary.wiley.com/terms-and-conditions) on Wiley Online Library for rules of use; OA articles are governed by the applicable Creative Commons License

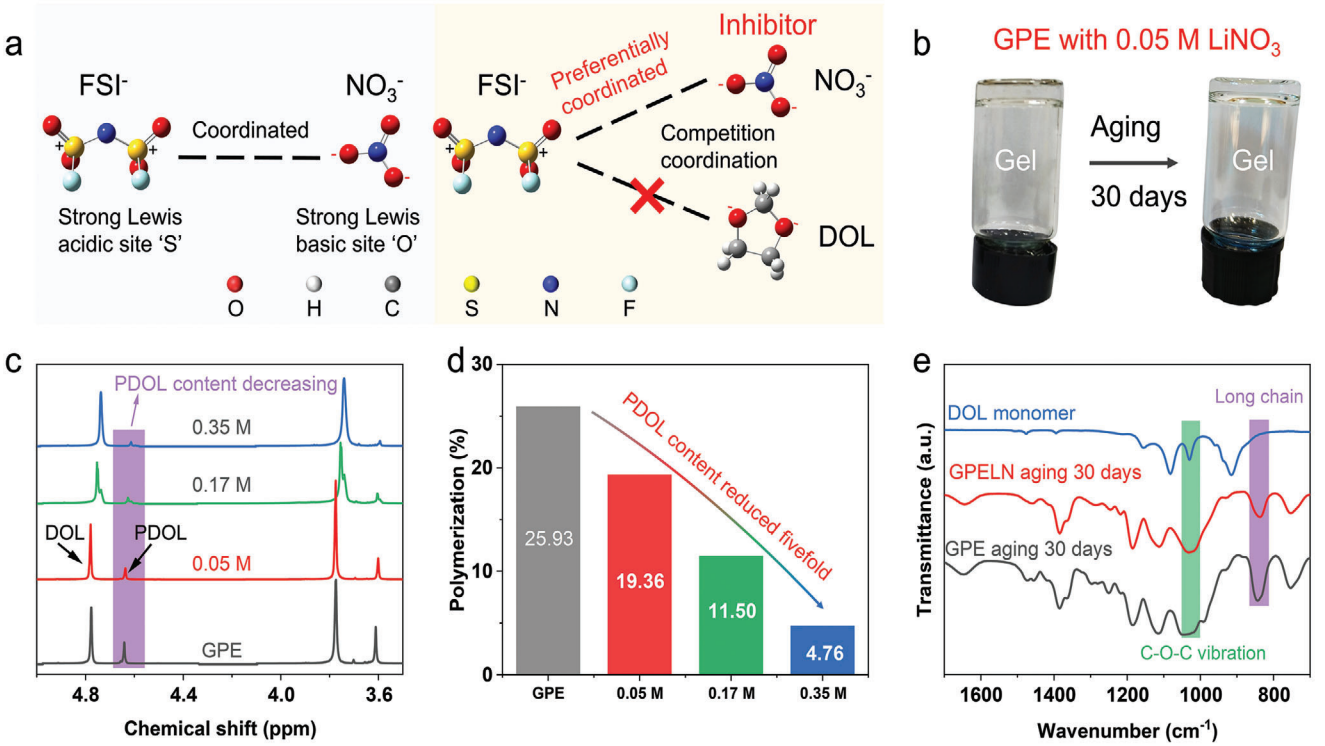

Figure 2. a) Schematic diagram of the interactions of FSI^- and NO_3^- and the competition coordination of DOL and NO_3^- for inhibiting the ring-opening polymerization of DOL. b) Optical images of GPELN (0.05 M $LiNO_3$ in GPE) after aging for 2 days and after aging for 30 days. c,d) ^1H NMR and corresponding polymerization ratio of GPE with various concentrations of $LiNO_3$ (aging two days). (e) FTIR spectra of GPE and GPELN after aging for 30 days.

polymerization of DOL. A stronger Lewis base will preferentially coordinate with the S atom in FSI^- instead of the O atom in the DOL,[22] thus blocking the attack on the O atom and controlling the polymerization of the DOL monomer in the LE. $LiNO_3$ has been widely used in lithium metal and lithium-sulfur batteries,[23] and NO_3^- can strongly coordinate with Li^+.[24] Therefore, the ESP of NO_3^- is calculated in Figure S9 (Supporting Information), and the electron of NO_3^- is mainly located on O atoms due to their strong electron absorption ability, which facilitates its coordination with strong Lewis acidic sites. The strong Lewis basic NO_3^- competes with DOL, preferentially coordinating with the S Lewis acidic site in FSI^-, which blocks the attack on the O atoms in DOL (**Figure** 2a). Thus, the partial FSI^- coordinated with NO_3^- does not trigger ring-opening polymerization of DOL, which leads to the reduction of intermediate-activated DOL molecules in GPELN, inhibiting the excessive polymerization of DOL and maintaining the stability of GPELN. (Figure S10, Supporting Information). Similarly, optical visualization experiments were also performed to verify the effect of $LiNO_3$ on inhibiting the evolution of GPE. As shown in Figure 2b, the LE with 0.05 M $LiNO_3$ (1 M LiFSI in DOL with 0.05 M $LiNO_3$) transforms into a clarified and transparent gel polymer electrolyte (GPELN) after aging for 2 days. Moreover, GPELN maintains this clarified and transparent gel state even after aging for 30 days, indicating stable physiochemical properties over time.

Further systematic investigation of $LiNO_3$ under various concentrations is studied based on the LE (1 M LiFSI in DOL), verifying this inhibitory effect of NO_3^- on ring-opening polymerization. As shown in ^1H-NMR (Figure 2c,d), GPE with $LiNO_3$ inhibitor exhibits a significant decrease in polymerization degree than that of GPE without $LiNO_3$,[25] and the content gradually decreases from 19.36% to 4.76% as $LiNO_3$ concentration increased from 0.05 to 0.35 M in LE, which strongly demonstrates that the inhibitory effect of NO_3^- can effectively inhibit the ring-opening polymerization of DOL. The ^1H-NMR was recorded after aging for 30 days in Figure S11 (Supporting Information), the peak of DOL nearly disappears in the GPE after aging 30 days (without $LiNO_3$), where PDOL content reaches up to 89.93%. In contrast, the peaks for both DOL and PDOL are still obvious in the GPELN after aging for 30 days with a content of ≈64.66% (Figure S11, Supporting Information). The smaller viscosity changes of GPELN compared with GPE indicate that $LiNO_3$ can effectively inhibit the ring-opening polymerization of DOL (Figure S12, Supporting Information). Figure 2e shows that the vibrational peaks of cyclic C—O—C almost disappear in GPE after aging for 30 days (without $LiNO_3$), indicating the completed conversion of DOL to PDOL. While, the cyclic C—O—C vibrational peaks of DOL monomer are still apparent in the GPELN after aging for 30 days, indicating the retention of DOL in the GPELN. These findings strongly demonstrate that the strong Lewis basic NO_3^- preferentially coordinates with the Lewis acidic site of S in the FSI^-, and the huge steric hindrance effect of NO_3^- can shield the interaction between DOL and FSI^-, inhibiting the undesirably ring-opening polymerization of DOL, preventing the transformation of LE to SPE and enhancing the stability of GPELN.

© 2024 The Author(s). Advanced Functional Materials published by Wiley-VCH GmbH

16163028, 0, Downloaded from https://onlinelibrary.wiley.com/doi/10.1002/adfm.202408525 by Karlsruher Institut F., Wiley Online Library on [01/08/2024]. See the Terms and Conditions (https://onlinelibrary.wiley.com/terms-and-conditions) on Wiley Online Library for rules of use; OA articles are governed by the applicable Creative Commons License

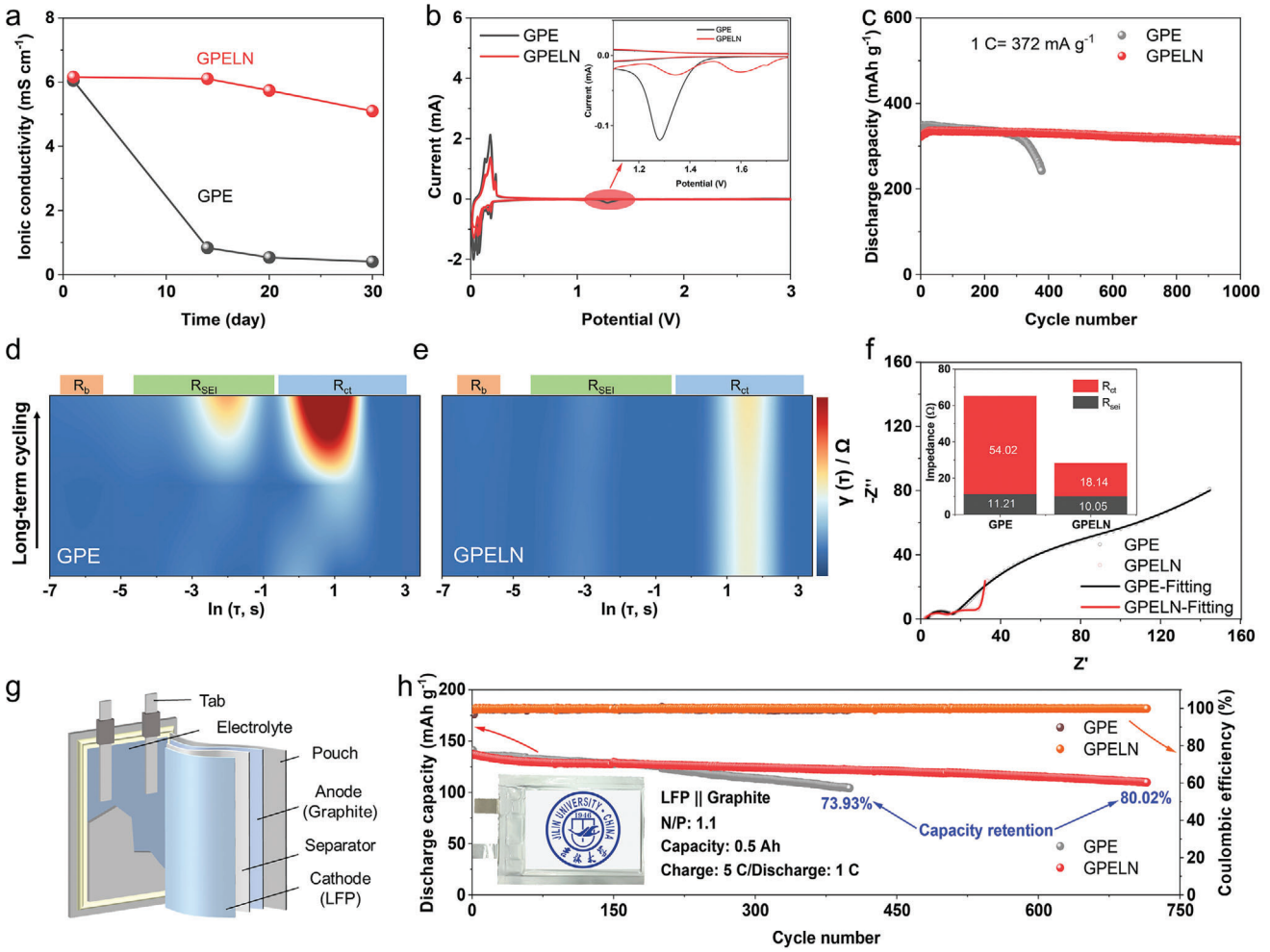

Figure 3. a) Ionic conductivity of GPE and GPELN with aging time. b) CV curves of GPE and GPELN. c) Cycling performance of graphite||Li half cell with GPE or GPELN at 5 C/1 C (discharge/charge), respectively. DRT analysis of the impedance data with different cycles for (d) GPE and (e) GPELN. f) EIS and corresponding fitting data of GPE and GPELN after cycling at 5 C/1 C (discharge/charge). g) Schematic diagram of the pouch full cell. h) Cycling performance of LFP||graphite pouch full cell in GPE and GPELN at 5 C/1 C (charge/discharge).

X-ray powder diffraction (XRD) and EIS are employed to reveal the changes in bulk electrolytes in GPE and GPELN. Figure S13 (Supporting Information) displays the GPE after aging for 30 days exhibits sharp diffraction peaks like the pure PDOL, implying the gradual transformation into SPE due to the continuous polymerization of DOL. Correspondingly, the Li^+ conductivity decreases from 6.05 (initial gel state) to 0.4 mS cm^{-1} (SPE after aging for 30 days) in **Figure 3a** and Figures S14 and S15 (Supporting Information). In contrast, GPELN reveals broad and amorphous diffraction peaks after aging for 30 days (Figure S13, Supporting Information), suggesting that $LiNO_3$ in the GPELN can effectively suppress the polymerization of DOL, maintaining an amorphous gel electrolyte over time. Thus, GPELN exhibits a significantly higher Li^+ conductivity (5.10 mS cm^{-1}) than that of GPE (0.40 mS cm^{-1}) (Figure 3a; Figure S15, Supporting Information), more than ten times higher. The Li^+ transfer number is recorded in Figure S16 (Supporting Information), both GPELN (0.70) and GPE (0.74) maintain high Li^+ transfer number,[26] indicating that a small amount of $LiNO_3$ has only a negligible effect on Li^+ transfer number. These results suggest that $LiNO_3$ can effectively inhibit the conversion of LE to SPE and maintain an amorphous gel electrolyte, thereby enhancing the Li^+ migration in GPELN.[14a] The linear sweep voltammetry (LSV) indicates the GPE and GPELN have a wide electrochemical stability window (3.96 V) in Figure S17 (Supporting Information). Cyclic voltammetry (CV) curves in Figure 3b reveal that GPELN can realize stable Li^+ intercalation and exhibits an extra reduction peak at 1.5 V, which is not observed in the GPE. This peak is attributed to the reduction of NO_3^- in the solvation structure,[27] which facilitates forming a stable and inorganic-rich SEI derived from anion to improve the stability of the interface.

The electrochemical performance is performed for graphite||Li half-cell with GPE and GPELN to investigate the inhibitory effect. The rate performance is displayed in Figure S18 (Supporting Information), the GPE and GPELN obtain similar discharge capacities at different current densities, higher than commercial carbonate electrolyte (EF), and the GPELN can slightly improve the initial coulombic efficiency due to the pre-reduction of

© 2024 The Author(s). Advanced Functional Materials published by Wiley-VCH GmbH

16163028, 0, Downloaded from https://onlinelibrary.wiley.com/doi/10.1002/adfm.202408525 by Karlsruher Institut F., Wiley Online Library on [01/08/2024]. See the Terms and Conditions (https://onlinelibrary.wiley.com/terms-and-conditions) on Wiley Online Library for rules of use; OA articles are governed by the applicable Creative Commons License

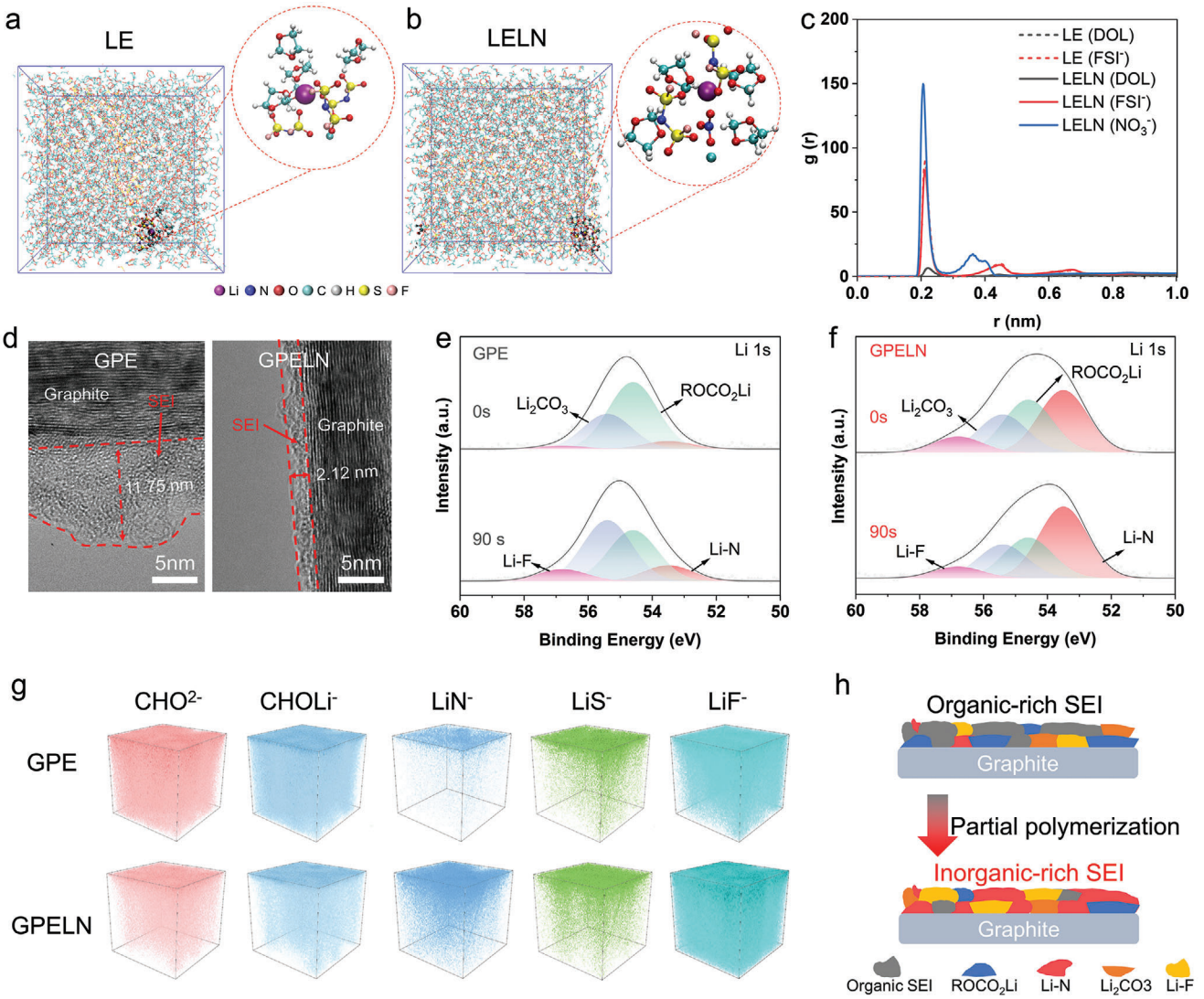

Figure 4. The snapshots from MD simulations for (a) LE (Liquid electrolyte: 1 M LiFSI in DOL) and b) LELN (LE with 0.1 M $LiNO_3$). c) The corresponding radial distribution function (RDF) obtained from MD simulations for LE and LELN. d) TEM results of SEI in GPE and GPELN. Li 1s XPS spectra of the SEI formed on electrodes in (e) GPE and (f) GPELN after various etching times. g) The 3D mapping reconstruction of organic and inorganic segments in GPE and GPELN by TOF-SIMS. h) Schematic diagram of the SEI in SPE and partial polymerization electrolyte (GPELN).

NO_3^- in the solvation structure (Figure S19, Supporting Information). The GPELN exhibits a smaller polarization and more stable cycling performance than that of GPE (Figure 3c and Figure S20, Supporting Information), and the GPELN has a higher capacity of 311.62 mAh g^{-1} after 1000 cycles at 5 C/1 C (discharge/charge) in Figure 3c, which demonstrates that the GPELN can improve the fast-charging cycling stability than the GPE (242.62 mAh g^{-1} after 388 cycles). The corresponding EIS and distribution of relaxation time (DRT) were recorded to evaluate the kinetic changes in GPE and GPELN during cycling. As depicted in Figure S22 (Supporting Information), the EIS resistance of GPE continuously increases with cycling, whereas the GPELN exhibits a neglectable increase. In detail, the R_{sei} (resistances of SEI) and R_{ct} (resistances of charge transfer) in GPE dramatically increase with the rapidly decreasing of fast-charging electrochemical performance (Figure 3d).[28] In contrast, GPELN exhibits neglectable changes in R_{sei} and R_{ct} during fast-charging cycling (Figure 3e) and a smaller R_{sei} and R_{ct} value than GPE after cycling (Figure 3f), which facilitates maintaining stable cycling performance and avoiding the generation of lithium dendrites under fast-charge conditions (Figure S23, Supporting Information). To evaluate practical applications, lithium iron phosphate (LFP)||graphite pouch full cell is assembled and tested (Figure 3g,h; Figure S24, Supporting Information). The GPELN maintains a capacity of 109.80 mAh g^{-1} after 715 cycles under the fast-charging rate of 5 C, corresponding to the capacity retention of 80.02% and energy density of 277.64 Wh Kg^{-1}, strongly evidencing the possibility for practical devices.

To further elucidate the effect of $LiNO_3$ on the solvation structure in GPE and GPELN, molecular dynamics (MD) simulations were operated (**Figure** 4a,b). Compared to the LE, the NO_3^- species integrate into the solvation structure. The

© 2024 The Author(s). Advanced Functional Materials published by Wiley-VCH GmbH

16163028, 0, Downloaded from https://onlinelibrary.wiley.com/doi/10.1002/adfm.202408525 by Karlsruher Institut F., Wiley Online Library on [01/08/2024]. See the Terms and Conditions (https://onlinelibrary.wiley.com/terms-and-conditions) on Wiley Online Library for rules of use; OA articles are governed by the applicable Creative Commons License

corresponding radial distribution functions (RDF) and coordination number (CN) witness the increased coordination peaks of NO_3^- around Li^+ (Figure 4c and Figure S25, Supporting Information),[25] which further supports the integration of NO_3^- into the solvation shell, facilitating a stable and inorganic-rich SEI formation. The transmission electron microscopy (TEM) images in Figure 4d also show the electrode with GPELN obtains a thin and homogeneous SEI with a thickness of 2.12 nm, much thinner than that in the GPE of ≈ 11.75 nm, indicating that GPELN can inhibit the continuous decomposition of electrolytes and maintain the stability of SEI during cycling. Additionally, the in-depth X-ray photoelectron spectroscopy (XPS) spectra of Li 1s at different etching times reveal a decrease in Li—N and Li—F inorganic complexes from the inner to the outer layers of SEI in GPE (Figure 4e),[29] while the presence of $LiCO_3$ and $ROCO_2Li$ increases (Figure S26, Supporting Information), which suggests that the PDOL is gradually formed by DOL polymerization. Conversely, GPELN exhibits higher ratios of inorganic components (Li—N and Li—F) and fewer organic components ($ROCO_2Li$) than that of GPE (Figure 4f), confirming anion decomposition on the graphite surface to form an inorganic and stable SEI, which is consistent with the above results of CV and MD. Time-of-flight secondary ion mass spectrometry (TOF-SIMS) provides a more intuitive and visual perspective to analyze this difference and discrepancy of SEI and interface in GPE and GPELN. As displayed in Figure 4g, CHO^{2-} segments signals, representing organic components, increase with etching time in the GPE, with a higher intensity than in GPELN. The corresponding 3D mapping reconstruction of organic CHO^{2-} and inorganic LiN^-, LiS^- and LiF^- segments reveals that GPELN contains more inorganic and less organic components than that of GPE in Figure 4 g and Figure S27 (Supporting Information). The uniformity of inorganic and organic components from the inner to the outer layers in the GPELN derived from anion (Figure 4h) is capable of keeping the stability of GPE and Li^+ migration from electrolyte bulk to interface, suggesting the fast-charging cycling stability in GPELN.

3. Conclusion

In summary, a strategy of gradient polymerization of forming GPE is pioneered, stabilizing the electrolyte/electrode interface with an accelerated Li^+ migration feature. As a demo, the inhibitor of $LiNO_3$ is proposed to effectively control the ring-opening polymerization of DOL and stabilize the gel structure of GPELN, accelerating the Li^+ migration and stabilizing the fast-charging cycling capability of graphite. Meanwhile, the mechanism of the inhibitor of strong Lewis acidic competitive reaction has been comprehensively investigated from electrochemical and spectroscopical measurement to the theoretical simulations. Moreover, the stable and inorganic-rich SEI derived from the inhibitor anion could enhance the stability of SEI in the GPELN. As a result, the as-prepared lithium iron phosphate (LFP)||graphite pouch full cell employed with GPELN stabilizes the capacity of 109.80 mAh g^{-1} at a fast-charging rate of 5 C, corresponding to the energy density of 277.64 Wh kg^{-1} after 715 cycles, providing new insights and a facile pathway to achieve fast-charging lithium-ion batteries.

Supporting Information

Supporting Information is available from the Wiley Online Library or from the author.

Acknowledgements

This work was supported by the National Natural Science Foundation of China (No. 51932003), the Fundamental Research Funds for the Central Universities, JLU (45122031B004), the Start-up research funding of Jilin University (419080523147), the Natural Science Foundation of Jiangsu Province (BK. 20210130). Dr. Jian Wang acknowledges the funding provided by the Alexander von Humboldt Foundation and the basic funding of the Helmholtz Association. The authors also thank the support from Nano-X, Suzhou Institute of Nano-tech and Nano-bionics, Chinese Academy of Sciences.

Open access funding enabled and organized by Projekt DEAL.

Conflict of Interest

The authors declare no conflict of interest.

Data Availability Statement

The data that support the findings of this study are available from the corresponding author upon reasonable request.

Keywords

fast charge, gel polymer electrolyte, inhibitory effect, in situ polymerization, Lithium-ion battery

Received: May 17, 2024
Revised: June 21, 2024
Published online:

[1] a) G. Zhang, J. Li, Q. Wang, H. Wang, J. Wang, K. Yu, J. Chang, C. Wang, X. Hong, Q. Ma, Y. Deng, *ACS Energy Lett.* **2023**, *8*, 2868; b) P. Jaumaux, J. Wu, D. Shanmukaraj, Y. Wang, D. Zhou, B. Sun, F. Kang, B. Li, M. Armand, G. Wang, *Adv. Funct. Mater.* **2021**, *31*, 2008644.
[2] a) L. Li, J. Liu, L. Li, J. Chen, J. Liu, R. Zhou, L. Zhang, *J. Energy Storage* **2024**, *87*, 111364; b) G. Jiang, J. Liu, Z. Wang, J. Ma, *Adv. Funct. Mater.* **2023**, *33*, 2300629.
[3] a) W. Feng, Y. Zhao, Y. Xia, *Adv. Mater.* **2024**, *36*, 2306111; b) H. Wan, Z. Wang, W. Zhang, X. He, C. Wang, *Nature* **2023**, *623*, 739; c) Y. J. Liu, R. Y. Fang, D. Mitlin, *Tungsten* **2022**, *4*, 316; d) C. Liao, C. Yu, S. Chen, C. Wei, Z. Wu, S. Chen, Z. Jiang, S. Cheng, J. Xie, *Renewables* **2023**, *1*, 266.
[4] Z. Wang, J. Xia, X. Ji, Y. Liu, J. Zhang, X. He, W. Zhang, H. Wan, C. Wang, *Nat. Energy* **2024**, *9*, 251.
[5] D. Lin, P. Y. Yuen, Y. Liu, W. Liu, N. Liu, R. H. Dauskardt, Y. Cui, *Adv. Mater.* **2018**, *30*, 1802661.
[6] J. Janek, W. G. Zeier, *Nat. Energy* **2023**, *8*, 230.
[7] T. T. Vu, H. J. Cheon, S. Y. Shin, G. Jeong, E. Wi, M. Chang, *Energy Storage Mater.* **2023**, *61*, 102876.
[8] a) F. N. Jiang, X. B. Cheng, S. J. Yang, J. Xie, H. Yuan, L. Liu, J. Q. Huang, Q. Zhang, *Adv. Mater.* **2023**, *35*, 2209114; b) S. J. Tan, J. Yue, Y. F. Tian, Q. Ma, J. Wan, Y. Xiao, J. Zhang, Y. X. Yin, R. Wen, S. Xin, Y. G. Guo, *Energy Storage Mater.* **2021**, *39*, 186.

© 2024 The Author(s). Advanced Functional Materials published by Wiley-VCH GmbH

16163028, 0, Downloaded from https://onlinelibrary.wiley.com/doi/10.1002/adfm.202408525 by Karlsruher Institut F., Wiley Online Library on [01/08/2024]. See the Terms and Conditions (https://onlinelibrary.wiley.com/terms-and-conditions) on Wiley Online Library for rules of use; OA articles are governed by the applicable Creative Commons License

[9] S. Huang, Z. Cui, L. Qiao, G. Xu, J. Zhang, K. Tang, X. Liu, Q. Wang, X. Zhou, B. Zhang, G. Cui, *Electrochim. Acta* **2019**, *299*, 820.
[10] Z. Zhang, X. Liu, D. Wang, H. Qin, X. He, B. Gao, G. Li, W. Zheng, Z. Zhuang, G. Yang, X. Ou, *Energy Storage Mater.* **2024**, *69*, 103419.
[11] a) F. Q. Liu, W. P. Wang, Y. X. Yin, S. F. Zhang, J. L. Shi, L. Wang, X. D. Zhang, Y. Zheng, J. J. Zhou, L. Li, Y. G. Guo, *Sci. Adv.* **2018**, *4*, eaat5383; b) B. Deng, M. X. Jing, R. Li, L. X. Li, H. Yang, M. Q. Liu, J. Xiang, W. Y. Yuan, X. Q. Shen, *J. Colloid Interface Sci.* **2022**, *620*, 199.
[12] N. W. Utomo, Y. Deng, Q. Zhao, X. Liu, L. A. Archer, *Adv. Mater.* **2022**, *34*, 2110333.
[13] a) G. Yang, W. Hou, Y. Zhai, Z. Chen, C. Liu, C. Ouyang, X. Liang, P. Paoprasert, N. Hu, S. Song, *EcoMat* **2023**, *5*, 12325; b) X. Peng, T. Wang, B. Liu, Y. Li, T. Zhao, *Energy Environ. Sci.* **2022**, *15*, 5350.
[14] a) Q. Zhao, X. Liu, J. Zheng, Y. Deng, A. Warren, Q. Zhang, L. Archer, *Proc. Natl. Acad. Sci. USA* **2020**, *117*, 26053; b) P. Cheng, H. Zhang, Q. Ma, W. Feng, H. Yu, X. Huang, M. Armand, Z. Zhou, *Electrochim. Acta* **2020**, *363*, 137198.
[15] a) C. Sun, X. Ji, S. Weng, R. Li, X. Huang, C. Zhu, X. Xiao, T. Deng, L. Fan, L. Chen, X. Wang, C. Wang, X. Fan, *Adv. Mater.* **2022**, *34*, 2206020; b) D. Xia, E. P. Kamphaus, A. Hu, S. Hwang, L. Tao, S. Sainio, D. Nordlund, Y. Fu, H. Huang, L. Cheng, F. Lin, *ACS Energy Lett.* **2023**, *8*, 1379; c) J. Wang, J. Zhang, J. Wu, M. Huang, L. Jia, L. Li, Y. Zhang, H. Hu, F. Liu, Q. Guan, M. Liu, H. Adenusi, H. Lin, S. Passerini, *Adv. Mater.* **2023**, *35*, 2302828; d) J. Wang, J. Yang, Q. Xiao, L. Jia, H. Lin, Y. Zhang, *ACS Appl. Mater. Interfaces* **2019**, *11*, 30500; e) J. Wang, L. Jia, J. Zhong, Q. Xiao, C. Wang, K. Zang, H. Liu, H. Zheng, J. Luo, J. Yang, H. Fan, W. Duan, Y. Wu, H. Lin, Y. Zhang, *Energy Storage Mater.* **2019**, *18*, 246.
[16] W. Ren, Y. Zhang, R. Lv, S. Guo, W. Wu, Y. Liu, J. Wang, *J. Power Sources* **2022**, *542*, 231773.
[17] H. Yang, B. Zhang, M. Jing, X. Shen, L. Wang, H. Xu, X. Yan, X. He, *Adv. Energy Mater.* **2022**, *12*, 2201762.
[18] J. Zhao, M. Li, H. Su, Y. Liu, P. Bai, H. Liu, L. Ma, W. Li, J. Sun, Y. Xu, *Small Methods* **2023**, *7*, 2300228.
[19] X. Y. Li, S. Feng, C. X. Zhao, Q. Cheng, Z. X. Chen, S. Y. Sun, X. Chen, X. Q. Zhang, B. Q. Li, J. Q. Huang, Q. Zhang, *J. Am. Chem. Soc.* **2022**, *144*, 14638.
[20] Y. Song, J. He, Y. Zhang, R. A. Gilsdorf, E. Y. X. Chen, *Nat. Chem.* **2023**, *15*, 366.
[21] X. Lu, Y. Wang, X. Xu, B. Yan, T. Wu, L. Lu, *Adv. Energy Mater.* **2023**, *13*, 2301746.
[22] a) Y. Liu, Y. Elias, J. Meng, D. Aurbach, R. Zou, D. Xia, Q. Pang, *Joule* **2021**, *5*, 2323; b) L. Zhou, F. Wang, F. Yang, X. Liu, Y. Yu, D. Zheng, X. Lu, *Angew. Chem., Int. Ed.* **2022**, *61*, 202208051.
[23] a) Q. Zhao, N. W. Utomo, A. L. Kocen, S. Jin, Y. Deng, V. X. Zhu, S. Moganty, G. W. Coates, L. A. Archer, *Angew. Chem., Int. Ed.* **2022**, *61*, 202116214; b) J. Wang, L. Jia, H. Liu, C. Wang, J. Zhong, Q. Xiao, J. Yang, S. Duan, K. Feng, N. Liu, W. Duan, H. Lin, Y. Zhang, *ACS Appl. Mater. Interfaces* **2020**, *12*, 12727; c) J. Wang, J. Zhang, Y. Zhang, H. Li, P. Chen, C. You, M. Liu, H. Lin, S. Passerini, *Adv. Mater.* **2024**, 2402792.
[24] C. Yan, Y. X. Yao, X. Chen, X. B. Cheng, X. Q. Zhang, J. Q. Huang, Q. Zhang, *Angew. Chem., Int. Ed.* **2018**, *57*, 14055.
[25] Y. Wang, T. Li, X. Yang, Q. Yin, S. Wang, H. Zhang, X. Li, *Adv. Energy Mater.* **2023**, *14*, 2303189.
[26] D. M. Pesko, S. Sawhney, J. Newman, N. P. Balsara, *J. Electrochem. Soc.* **2018**, *165*, A3014.
[27] S. Stuckenberg, M. M. Bela, C. T. Lechtenfeld, M. Mense, V. Küpers, T. T. K. Ingber, M. Winter, M. C. Stan, *Small* **2024**, *20*, 2305203.
[28] J. Chen, E. Quattrocchi, F. Ciucci, Y. Chen, *Chem* **2023**, *9*, 2267.
[29] D. Luo, L. Zheng, Z. Zhang, M. Li, Z. Chen, R. Cui, Y. Shen, G. Li, R. Feng, S. Zhang, G. Jiang, L. Chen, A. Yu, X. Wang, *Nat. Commun.* **2021**, *12*, 186.

© 2024 The Author(s). Advanced Functional Materials published by Wiley-VCH GmbH

16163028, 0, Downloaded from https://onlinelibrary.wiley.com/doi/10.1002/adfm.202408525 by Karlsruher Institut F., Wiley Online Library on [01/08/2024]. See the Terms and Conditions (https://onlinelibrary.wiley.com/terms-and-conditions) on Wiley Online Library for rules of use; OA articles are governed by the applicable Creative Commons License